Sexual dimorphism of niche architecture and regulation of the *Caenorhabditis elegans* germline stem cell pool

Sarah L. Crittenden[a,b], ChangHwan Lee[a,b], Ipsita Mohanty[b,†], Sindhu Battula[b], Karla Knobel[b,‡], and Judith Kimble[a,b,*]

[a]Howard Hughes Medical Institute and [b]Department of Biochemistry, University of Wisconsin–Madison, Madison, WI 53706

ABSTRACT **Stem cell maintenance by niche signaling is a common theme across phylogeny. In the *Caenorhabditis elegans* gonad, the broad outlines of germline stem cell (GSC) regulation are the same for both sexes: GLP-1/Notch signaling from the mesenchymal distal tip cell niche maintains GSCs in the distal gonad of both sexes and does so via two key stem cell regulators, SYGL-1 and LST-1. Yet most recent analyses of niche signaling and GSC regulation have focused on XX hermaphrodites, an essentially female sex making sperm in larvae and oocytes in adults. Here we focus on GSC regulation in XO males. Sexual dimorphism of niche architecture, reported previously, suggested that the molecular responses to niche signaling or numbers of GSCs might also be sexually distinct. Remarkably, this is not the case. This work extends our understanding of the sexually dimorphic niche architecture, but also demonstrates that the dimorphic niches drive a similar molecular response and maintain a similar number of GSCs in their stem cell pools.**

Monitoring Editor
Yukiko Yamashita
University of Michigan

Received: Mar 19, 2019
Revised: Apr 24, 2019
Accepted: May 2, 2019

INTRODUCTION

In intact organisms, stem cells are maintained within a niche, a site that promotes their naïve stem cell–like state and prevents differentiation (Lander *et al.*, 2012). Niches are thus crucial for tissue development and homeostasis with implications for wound repair, regeneration, and cancer. Among the many niches identified, differences are striking: niches differ in architecture—the number, shape and type of cells, or extracellular matrix—and they differ in the molecular mechanisms used for stem cell control—the number and type of signaling pathways used to communicate with stem cells (e.g., Jones and Wagers, 2008). Understanding the significance of these differences, however, remains a challenge.

The *Caenorhabditis elegans* mesenchymal niche for germline stem cells (GSCs) has served as a paradigm for stem cell regulation for nearly 40 yr. Here we focus on the sexual dimorphism of this niche to ask how differences influence stem cell regulation. In both sexes (Figure 1, A and B), the niche maintains GSCs within a progenitor zone (PZ) of ~225 germ cells, GSCs divide stochastically, and GSC daughters mature as they move along the distal to proximal axis (Crittenden *et al.*, 2006; Morgan *et al.*, 2010; Rosu and Cohen-Fix, 2017). Also in both sexes, the niche relies on GLP-1/Notch signaling to maintain GSCs (Austin and Kimble, 1987) (Figure 1C); niche signaling activates the same two target genes, *lst-1* and *sygl-1*, in GSCs (Kershner *et al.*, 2014), and GSC self-renewal relies on the same major regulators—two PUF RNA-binding proteins, FBF-1 and FBF-2, and their key cofactors, LST-1 and SYGL-1 (Crittenden *et al.*, 2002; Shin, Haupt, *et al.*, 2017) (Figure 1D). Thus, the regulatory landscape is strikingly similar in the sexes.

Yet there are differences. The hermaphrodite niche consists of a single distal tip cell (hDTC) that caps the end of the hermaphrodite PZ (hPZ) (Figure 1A), whereas the male niche consists of two DTCs

This article was published online ahead of print in MBoC in Press (http://www.molbiolcell.org/cgi/doi/10.1091/mbc.E19-03-0164) on May 8, 2019.

Present addresses: [†]Duke Human Vaccine Institute, Durham, NC 27710; [‡]Waisman Center, University of Wisconsin–Madison, Madison, WI 53705.

*Address correspondence to: Judith Kimble (jekimble@wisc.edu).

Abbreviations used: ATS, active transcription site; DTC, distal tip cell; gcd, germ cell diameters; GFP, green fluorescent protein; GSC, germline stem cell; hPZ, hermaphrodite progenitor zone; mDTC, male distal tip cell; PBS, phosphate-buffered saline; PZ, progenitor zone; smFISH, single molecule fluorescence in situ hybridization.

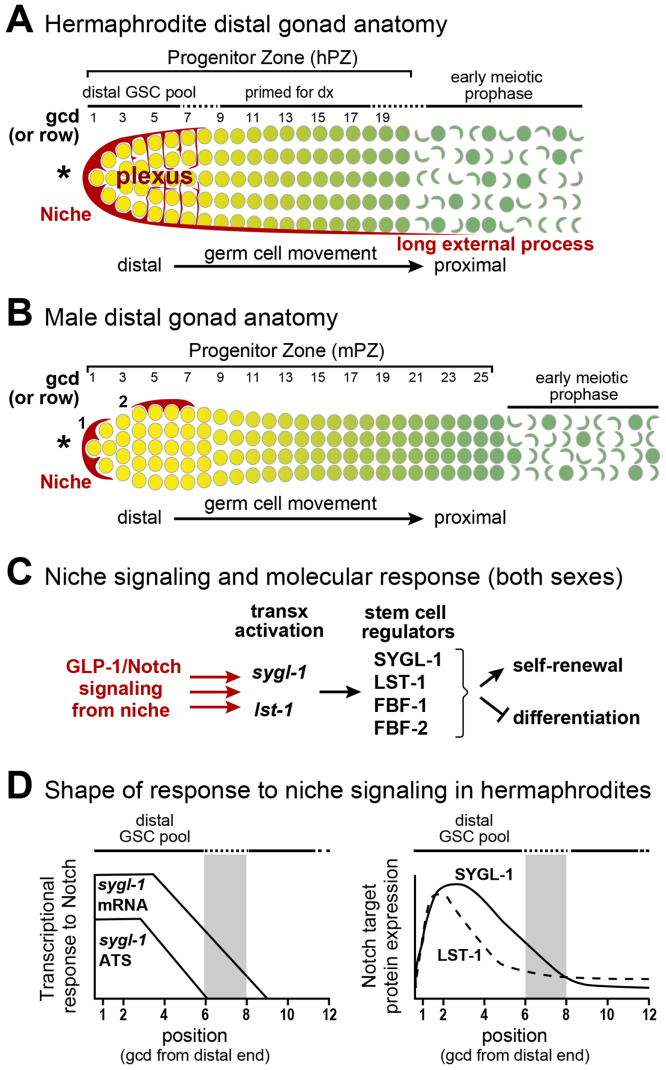

FIGURE 1: Hermaphrodite and male DTC niches and PZs (PZs). (A, B) Diagrams of the distal gonads of each sex, each with a mesenchymal niche (red) and a germline PZ with ~225 germ cells that develop as they move from distal to proximal along the gonadal axis (yellow to green). Germ cell position is conventionally described as the number of germ cell diameters (gcd) from the distal end, with rows of germ cells at each position. Germ cells are depicted at the gonad periphery; not shown is the central rachis of cytoplasm to which all germ cells connect via bridges (Hirsh *et al.*, 1976; Amini *et al.*, 2014; Seidel *et al.*, 2018). Although germ cells are connected through the rachis, each is partially enclosed by plasma membrane and functions largely autonomously with respect to cell cycle stage; for simplicity, the convention is to call them germ cells. Also not shown are germline folds in the hermaphrodite PZ (Raiders *et al.*, 2018; Seidel *et al.*, 2018). Here and in all figures, an asterisk marks the distal end. (A) Hermaphrodite distal gonad. The hDTC cell body caps distal germ cells and extends a plexus of processes that contact most germ cells through rows 6–8 (Byrd *et al.*, 2014; Lee *et al.*, 2016). The hPZ has fewer cells per row distally and then widens (Morgan *et al.*, 2010); it extends ~20 gcd from the distal end. The hPZ contains a distal pool of naïve, stem cell–like undifferentiated cells (yellow), and a proximal pool of cells that are primed for differentiation and mature progressively (graded green) as they move proximally (darker green) (Cinquin, Crittenden, *et al.*, 2010; Fox *et al.*, 2011). (B) Male distal gonad. One mDTC typically resides at the distal end and the other on the dorsal side. We refer to the dorsal mDTC as lateral since in extruded gonads its dorsal, lateral, or ventral position cannot be determined. The mPZ bulges distally and then becomes thinner, extending ~25 gcd from the distal end (Morgan *et al.*, 2010). Other features shown for the hermaphrodite distal gonad (e.g., distal and proximal pools) were not known prior this work. Here and in all figures, the position of most-distal male DTC is marked 1 and the lateral DTC is marked 2. (C) Molecular stem cell regulation. The niche uses GLP-1/Notch signaling to activate transcription of the *sygl-1* and *lst-1* genes in GSCs (Kershner *et al.*, 2014; Lee *et al.*, 2016). The SYGL-1 and LST-1 proteins work with FBF-1 and FBF-2 to promote self-renewal and inhibit differentiation (Shin, Haupt, *et al.*, 2017). (D) Hermaphrodite GSC response to GLP-1/Notch signaling, based on previous reports (Lee *et al.*, 2016; Shin, Haupt, *et al.*, 2017). Left, *sygl-1* ATS reveal the direct response to signaling; *sygl-1* mRNAs extend more proximally than ATS. Both ATS and mRNAs are restricted to the GSC pool region and are graded. Right, SYGL-1 (solid line) and LST-1 (dashed line) proteins are restricted to the GSC pool region and graded. Gray bar indicates the estimated proximal boundary of the GSC pool (6–8 gcd; Cinquin, Crittenden, *et al.*, 2010).

(mDTCs) that reside at or near the end of the male PZ (mPZ) (Figure 1B) (Kimble and White, 1981; Morgan *et al.*, 2010). Critical to this analysis, the mDTCs are positioned asymmetrically, which might be expected to generate an asymmetric response among GSCs. In addition to these niche differences, the PZ is narrower and longer in males than hermaphrodites, germ cell cycles are faster in males (Morgan *et al.*, 2010), and the hPZ is folded whereas the mPZ is not (Raiders *et al.*, 2018; Seidel *et al.*, 2018). Therefore, both the niches and PZs are sexually dimorphic.

The germline response to GLP-1/Notch signaling has been analyzed primarily in hermaphrodites. One key finding was that GLP-1/Notch signaling patterns the hPZ into distal and proximal regions (Figure 1A) (Cinquin, Crittenden, *et al.*, 2010). Germ cells in roughly the distal third of the hPZ are maintained in a stem cell–like state and share several features: they have similar cell cycle rates (Crittenden *et al.*, 2006; Fox *et al.*, 2011; Rosu and Cohen-Fix, 2017), they block in an undifferentiated state upon cell cycle arrest (Cinquin, Crittenden, *et al.*, 2010; Jeong *et al.*, 2011), and they express high levels of self-renewal markers LST-1 and SYGL-1 (Kershner *et al.*, 2014; Shin, Haupt, *et al.*, 2017) but low levels of differentiation markers (Cinquin, Crittenden, *et al.*, 2010; Fox *et al.*, 2011). By contrast, germ cells in the proximal pool have left the stem cell state and begun the path toward differentiation: they have fewer mitotic divisions, enter into meiotic prophase upon cell cycle arrest, and express low levels of self-renewal markers and high levels of differentiation markers (Crittenden *et al.*, 2006; Cinquin, Crittenden, *et al.*, 2010; Fox *et al.*, 2011; Rosu and Cohen-Fix, 2017). The distal GSC and proximal pools within the hPZ are therefore well established, but the existence of similar pools in males had not been tested.

To learn how the hPZ is patterned, more recent studies assessed the hDTC architecture (Byrd *et al.*, 2014; Linden *et al.*, 2017) and the shape of the molecular response to GLP-1/Notch signaling (Kershner *et al.*, 2014; Lee *et al.*, 2016; Shin, Haupt, *et al.*, 2017). Understanding hDTC architecture provides insight into where signaling may occur, because the hDTC expresses ligands for GLP-1/Notch signaling, LAG-2 and APX-1 (Henderson *et al.*, 1994; Nadarajan, Govindan, *et al.*, 2009). A myristoylated green fluorescent protein (GFP) expressed under control of a *lag-2* promoter revealed that the hDTC cell body extends two types of cytoplasmic processes (Figure 1A): an elaborate plexus of fine processes that intercalates in and around most germ cells in the region corresponding to the distal pool (Byrd *et al.*, 2014; Lee *et al.*, 2016; Linden *et al.*, 2017) and long

external processes that extend beyond the hPZ and do not correlate with germ cell fate (Crittenden *et al.*, 2006; Byrd *et al.*, 2014). Notch signaling acts between cells (e.g., DTC and germ cell), and the existence of the hDTC plexus suggests that GLP-1/Notch signaling acts directly on germ cells throughout the distal region and thus at some distance from the DTC cell body. The shape of the molecular response to GLP-1/Notch signaling provides clues about where signaling actually occurs. Visualization of Notch-dependent transcription with single molecule fluorescence in situ hybridization (smFISH) reveals a direct readout of active signaling. Importantly, that active signaling was found throughout the distal pool and was graded, with the highest response in germ cells adjacent to the DTC (Figure 1D) (Lee *et al.*, 2016). Expression of Notch-dependent mRNAs and proteins shows where these key regulators exist and could be functioning. In hermaphrodites, the *sygl-1* and *lst-1* mRNAs and proteins are restricted to the distal pool and graded, though less steeply (Figure 1D) (Kershner *et al.*, 2014; Lee *et al.*, 2016; Shin, Haupt, *et al.*, 2017). These findings led to the hypothesis that at least three factors are relevant to the establishment of the hPZ distal GSC pool: extent of the hDTC plexus (Byrd *et al.*, 2014), extent of the graded transcriptional response (Lee *et al.*, 2016), and extent of *sygl-1* RNA and protein (Lee *et al.*, 2016; Shin, Haupt, *et al.*, 2017).

In this paper, we ask how a sexually dimorphic niche affects PZ patterning. To this end, we investigate the fine architecture of the male DTCs, the existence of patterned pools within the mPZ, and the shape of the GSC molecular response to niche signaling. We confirm and extend our understanding of sexually dimorphic niche architecture and learn that the niches in the two sexes establish a remarkably similar pattern and drive a similarly graded molecular response.

RESULTS

Architecture of the DTC niche in males

We employed the *arg-1* promoter to visualize mDTCs. Past experiments used the *lag-2* promoter, which gives a strong signal in hDTCs but only a faint signal in mDTCs (Morgan *et al.*, 2010; Byrd *et al.*, 2014). The *arg-1* promoter, by contrast, gives a strong signal in mDTCs, but no signal in hDTCs (this paper; Sallee, Littleford, *et al.*, 2017). Expression of *arg-1* is therefore strikingly dimorphic. To ask whether *arg-1* regulates GSCs, we conducted genetic tests that revealed effects for five different DSL ligands, including *arg-1*. Their effects were mild, even in double mutants, suggesting considerable redundancy (Table 1). A full understanding of DSL ligands in the male gonad is beyond the scope of this work.

As a reporter, we employed either cytoplasmic GFP (Kostas and Fire, 2002; Zhao *et al.*, 2007) or GFP with a membrane-targeting myristoylation sequence (myrGFP) in mDTCs and obtained similar results with both markers. We first scored positions of the two mDTC cell bodies along the distal-proximal axis in young adult males (Figure 2, A and D). Most gonads (43/50) had one mDTC at the distal end and one on the side of the gonad tube, as previously reported (Kimble and White, 1981; Morgan *et al.*, 2010). In a few cases, the two mDTCs were at the same point along the distal to proximal axis, either at the end (4/50) or on the side of the tube (3/50). When assessed in intact animals, we found that the mDTC on the side of the tube was typically dorsal (90%, $n = 20$). Since most experiments reported in this work used fixed extruded gonads (e.g., smFISH), we refer to the mDTC located on the side of the gonad as lateral, because its position as dorsal or ventral cannot be determined in fixed samples.

We next scored the extent of mDTC cell bodies along the distal-proximal axis. For this and other analyses in this work, we use the conventional metric of germ cell diameters (gcd) along the axis, sometimes referred to as germ cell rows along the axis. Each mDTC cell body covered 3–5 gcd or rows along the distal-proximal axis ($n = 35$; Figure 2A), and the two together cover 6–10 gcd on average (Figure 2, A and D). Finally, we scored cytoplasmic processes that extend from the mDTC cell body. In contrast to the hDTC (Figure 1A), most mDTCs lack a plexus (48/50) and most lack long external processes (31/50). However, most mDTCs do extend short processes between germ cells (42/50) (Figure 2C). The cell bodies and processes from the two mDTCs did not overlap extensively and were often in different z-planes of the gonad tube (Figure 2, A, B, and D). The lack of a plexus in males coupled with the lateral position of one mDTC result in little or no detectable contact between the mDTC niche and germ cells on one side of most male gonads (27/39 [70%]) (Figure 2, A–D; also see Figure 5, B and E, later in this article). The male niche is therefore strikingly asymmetric compared with the hermaphrodite niche.

Another difference in niche architecture is developmental: hDTCs develop their plexus soon after molting from the fourth larval stage into adulthood (Byrd *et al.*, 2014; Linden *et al.*, 2017). By contrast, mDTC architecture is similar in L4s ($n = 10$), young adults 1 d after L4 (A24, $n = 50$), and adults 2 d after L4 (A48, $n = 6$). At all stages, mDTCs cap adjacent germ cells, extend short processes, lack an extensive plexus, and can extend long external processes. We did observe two differences in older males: mDTC cell bodies elongated and 80% of animals had long external processes compared with 40% in L4 and young adults. In conclusion, niche architecture is sex-specific with respect to the number and position of DTCs as well as the extent and developmental regulation of niche processes.

Genotype[a]	PZ length (range)	*N*
Wild type	24 (20–28)	21
lag-2/+	19 (13–24)[b]	24
apx-1	18 (16–20)[b]	15
arg-1/0	23 (16–28)	21
dsl-1	17 (11–24)[b]	22
dsl-4/0	23 (14–33)	21
lag-2/+; +/apx-1	18 (11–25)[b]	23
lag-2/+; arg-1/0	19 (10–25)[c]	20
dsl-1; lag-2/+	19 (13–24)	11
apx-1; arg-1/0	14 (11–16)[d]	10

[a]Some strains included a P*lag-2*::GFP transgene. PZ lengths of animals either homozygous or heterozygous for the transgene were not significantly different from wild type. For complete genotypes of all strains, see *Materials and Methods*.
[b]Significantly different from wild type ($p < 0.001$).
[c]Significantly different from *arg-1/0* ($p < 0.001$).
[d]Significantly different from *apx-1* and *arg-1/0* ($p < 0.001$).

TABLE 1: PZ lengths of DSL ligand mutant males.

The male PZ is patterned with distal GSC and proximal pools

To ask whether the mPZ, like the hPZ, contains a distal GSC pool and a proximal pool that is primed for differentiation, we used the *emb-30* assay (Figure 3). The *emb-30* gene is required for progression from metaphase to anaphase during M-phase (Furuta *et al.*, 2000); without *emb-30*, germ cell cycling stops and the distal to

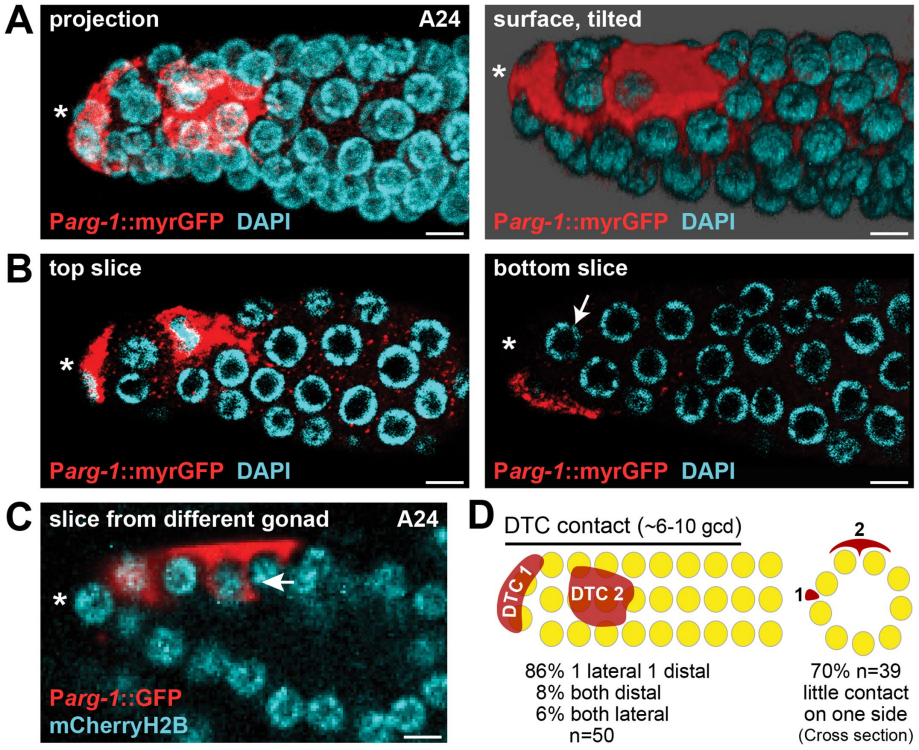

FIGURE 2: Architecture of male DTC and its processes. mDTCs are labeled with P*arg-1*::myrGFP (red); all nuclei are stained with DAPI (cyan). (A) Projected confocal z stack of a representative adult (A24) male gonad. mDTCs are either distal or lateral. The projection (left) shows all detectable mDTC signals in a single plane. Right: Surface rendering of the same gonad, tilted to show another view of mDTC contact with germ cells. (B) Comparison of top (left) and bottom (right) slices of the gonad in A show that mDTC contact is not uniform around the germline tube. The bottom slice (right) reveals germ cells with no detectable contact with mDTC processes (arrow) even in the distal-most PZ. (C) A different male gonad showing a lateral mDTC with short intercalating processes that embrace adjacent germ cells (arrow). About 85% of gonads ($n = 50$) have similar short processes that embrace adjacent germ cells. (D) Summary diagrams of mDTC position from side (left) or cross-section (right). Distal DTC is DTC 1, lateral DTC is DTC 2. The percentage of gonads with the various configurations is provided at the bottom. The cross-section represents the middle of DTC 2 and illustrates the lack of detectable DTC contact on one side of the gonad. Scale bars, 4 μm. *Distal end.

proximal movement of germ cells halts, allowing germ cells to reveal their developmental state in place (Figure 3A). In hermaphrodites, this assay revealed distal GSC and proximal pools within the PZ (see *Introduction*; Figure 1A). Thus, germ cells in the distal pool arrested in mitotic M-phase (PH3-positive) and expressed the differentiation marker GLD-1 at a very low or undetectable level, while germ cells in the proximal pool entered meiotic prophase and expressed high GLD-1 (Cinquin, Crittenden, *et al.*, 2010; Shin, Haupt, *et al.*, 2017).

To investigate the possibility of similar patterning in the male PZ, we first conducted a time course to learn whether and when the distal and proximal pools resolve after the temperature shift (Figure 3B). We raised *emb-30(ts)* males at permissive temperature until the L4 stage, then switched them to restrictive temperature and scored the position of PH3-positive cells and early meiotic prophase after 0, 8, 10, 12, and 15 h. After 12 h, a boundary had stabilized between undifferentiated distal and differentiated proximal germ cells (Figure 3B). We then used this 12-h time point to measure extents of the two pools with PH3 staining to mark cells arrested in mitosis and GLD-1 staining to mark differentiating cells. The distal pool extended an average of 7 gcd from the distal end (range 4–10 gcd, $n = 8$) and contained an average of 28 germ cells (range 17–34, $n = 8$). This extent and cell number were similar to those in hermaphrodites assayed in parallel (Figure 3D). We conclude that the mPZ, like the hPZ, is patterned and that sizes of the distal GSC pools are similar in the two sexes.

Male transcriptional response to GLP-1/Notch signaling is graded and restricted to distal GSC pool

We next visualized the *sygl-1* transcriptional response to GLP-1/Notch signaling in male GSCs and compared it to that response in hermaphrodite GSCs. For this analysis, we scored both active transcription sites (ATS) within nuclei, a direct readout of productive GLP-1/Notch signaling, and *sygl-1* mRNAs in the cytoplasm. A previous analysis in hermaphrodites revealed that *sygl-1* transcriptional activation is probabilistic and steeply graded within the distal pool region (Lee *et al.*, 2016).

To test the male response, we used *sygl-1* smFISH to see ATS and cytoplasmic mRNAs using a combination of intron-specific and exon-specific probes (Figure 4A). ATS and mRNAs were identified by established criteria (Lee *et al.*, 2016, 2017). Thus, ATS were found by colocalization of exon and intron probes as well as nuclear location, assessed by 4′,6-diamidino-2-phenylindole (DAPI). Mature, cytoplasmic mRNAs were found using signal from exon probes alone and location outside the nucleus (Figure 4A). Three features were obvious without quantitation. First, both ATS and mRNAs were spatially restricted within the PZ, and as in hermaphrodites, their extent correlated roughly with the extent of the GSC pool. Second, occurrence of ATS was probabilistic in males as it was in hermaphrodites. Third, *sygl-1* was not transcribed in the male proximal germline, where spermatogenesis occurs; by contrast, *sygl-1* was transcribed in the hermaphrodite proximal germline, where oogenesis occurs, albeit in a GLP-1-independent manner (see Figure 7, A and D, later in this article) (Kershner *et al.*, 2014; Lee *et al.*, 2016).

To quantitate the GLP-1/Notch transcriptional response, we used the MATLAB code that had been developed previously to analyze smFISH in hermaphrodites (Lee *et al.*, 2016, 2017) with modifications (see *Materials and Methods*). We focused on *sygl-1* ATS as a direct readout of GLP-1/Notch transcriptional activity. The ATS patterns were similarly graded in the two sexes, but not identical (Figure 4B, blue vs. gray bars). Thus, ATS extended more proximally in males than in hermaphrodites (Figure 4B, dotted lines). In addition, the percentage of ATS-positive nuclei were graded from ~45% at the distal end to ~5% at the proximal end, while in hermaphrodites, they were graded from ~65% to ~5% (Figure 4B). Thus, the male response is lower than hermaphrodite in the distal 1–2 gcd, but is higher 5–8 gcd from the distal end (Figure 4B). Distal germ cell nuclei were more likely to contain greater than one ATS per nucleus than were more proximal nuclei in both sexes (Figure 4C). As a

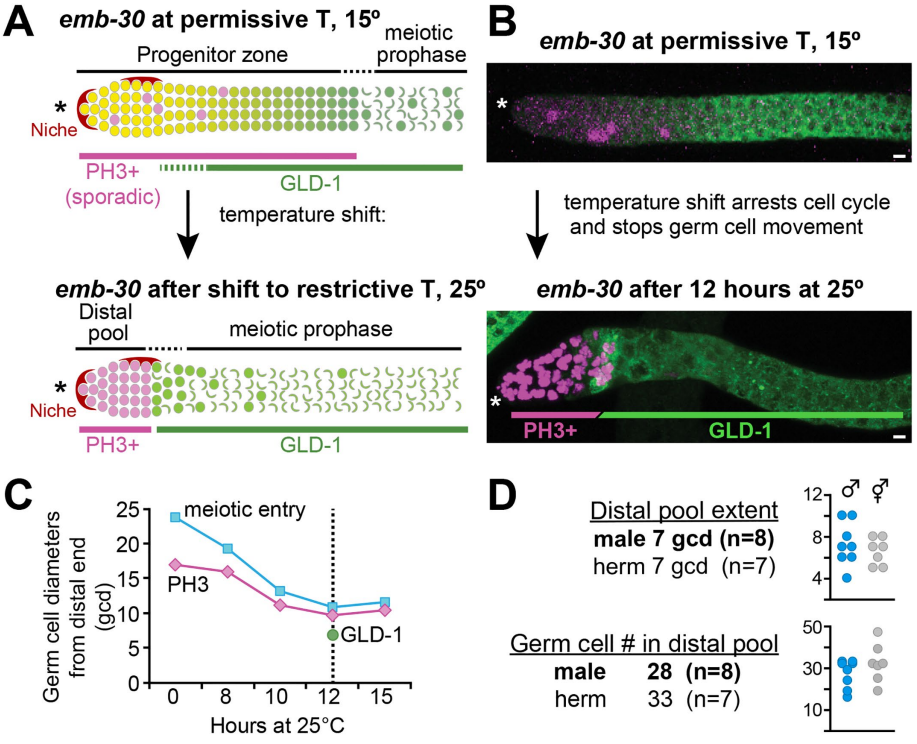

FIGURE 3: Patterning of developmental state in mPZ. (A, B) Anti-PH3 (magenta) detects germ cells in mitotic M-phase (Hendzel *et al.*, 1997); anti-GLD-1 (green) detects differentiating germ cells (Brenner and Schedl, 2016). (A) The *emb-30* assay to reveal mPZ patterning of cell state. At permissive temperature (top), germ cells in mitotic M-phase (PH3+) occur sporadically throughout the PZ, but after a shift to restrictive temperature (bottom), they are restricted to the distal part of the gonad. (B) Representative confocal projections of *emb-30* male germlines at permissive temperature (top) and after 12 h at restrictive temperature (bottom). (C) Summary of *emb-30* shift results. *x*-axis, time after shift to restrictive temperature; *y*-axis, distal-proximal distance. The positions of both PH3-positive (magenta line) and meiotic entry (cyan) become more distal with time, plateauing at ~12 h (dotted line). The boundary between low and high GLD-1 (green dot) after 12 h at restrictive temperature is indicated. (D) GSC pool characteristics were measured at the 12-h time point. The table shows averages; individual data points are shown in graphs. Males and hermaphrodites were done in parallel. *Distal end.

control, we assayed ATS of the nontarget gene, *let-858*, which is widely expressed in the germline (Kelly *et al.*, 1997; Lee *et al.*, 2016), and found that the percentage of cells with ATS is similar in both sexes (Figure 4D). We finally assessed ATS intensities and found a minimal difference between the sexes for *sygl-1* and no difference between the sexes for *let-858* (Figure 4, G and H). We conclude that the active transcriptional response to GLP-1/Notch signaling is restricted to the GSC pool and graded in both sexes, but that there are minor sex-specific differences in the shape of the response.

We next compared the abundance of *sygl-1* mature cytoplasmic mRNA in males and hermaphrodites. We first determined the percentage of cells possessing *sygl-1* mRNA above basal levels by estimating cell boundaries computationally and quantitating mRNA within those boundaries (Lee *et al.*, 2016) (Figure 4E). In males, cells with *sygl-1* mRNA levels above basal levels were restricted to a region 1–45 µm (~1–10 gcd) from the distal end (Figure 4, E and F), and the percentage of these cells was graded from ~80% at the distal-most end to ~5% more proximally. In hermaphrodites, cells with *sygl-1* mRNA above basal levels were restricted to a region 1–40 µm (~1–9 gcd) from the distal end, and the percentage of those cells was also graded (~98% at the distal-most end to ~5% at 40 µm). Therefore, as was shown previously in hermaphrodites (Lee *et al.*, 2016), the mRNA response is expanded proximally relative to ATS in males (compare Figure 4, B with E). We also compared the number of mRNAs per cell in males and hermaphrodites. Males had fewer mRNAs per cell than hermaphrodites in the distal 1–3 gcd and more mRNAs per cell more proximally, 5–11 gcd from the distal end (Figure 4F). In conclusion, as for ATS distribution, the mRNA response was restricted to and graded through the GSC pool, but there are sex-specific differences: the male response was lower in distal germ cells and higher in proximal germ cells.

Male DTCs and their association with *sygl-1* ATS-positive germ cells

Contacts between the mDTCs and germ cells are strikingly asymmetric and much less extensive in males than in hermaphrodites (Figure 2). These differences allowed us to investigate the relationship between germ cell proximity to the niche and the probability of Notch-dependent transcriptional activation. We quantitated mDTC contact and ATS state (ATS-positive or ATS-negative) in the same samples (Figure 5, A–C). To this end, we visualized the *sygl-1* transcriptional response with smFISH in gonads from animals carrying P*arg-1*::myrGFP to see mDTCs and their processes (Figure 5A). By eye, many *sygl-1* ATS-positive germ cells lacked contact with mDTCs though extensive contact with ATS-positive cells could also be seen (Figure 5A). With MATLAB, we assessed the percentage of germ cells contacting mDTCs in the distal-most 60 µm of the germline (Figure 5B). On average, ~40% of these germ cells have mDTC contact in the distal 1–2 gcd, ~65–70% have contact 2–5 gcd from the distal end and 20–30% have contact 8–9 gcd from the distal end. By contrast, in hermaphrodites ~99% of all germ cells contact the hDTC in the distal 1–2 gcd, ~70–85% have contact 2–5 gcd from the distal end, and ~60% have contact 7–8 gcd from the distal end (Lee *et al.*, 2016). We next quantitated the percentages of ATS-positive and ATS-negative cells with mDTC contact and found that on average, ~55% of ATS-positive germ cells contact an mDTC (Figure 5C). The percentage of ATS-positive cells without mDTC contact varies from gonad to gonad, but the majority of gonads have 20% or more ATS-positive cells with no detectable mDTC contact. This percentage is strikingly lower than in hermaphrodites, where essentially all (99%) ATS-positive germ cells were in contact with the hDTC (Lee *et al.*, 2016). Thus, while many ATS-positive germ cells contact an mDTC, many do not (Figure 5, A and C), indicating that GLP-1/Notch transcriptional activation can occur in the absence of detectable DTC contact in males.

SYGL-1 and LST-1 proteins are restricted in the male distal germline to the GSC pool

To ask whether SYGL-1 and LST-1 expression is similar in the distal gonads of the two sexes, we stained epitope-tagged SYGL-1 and LST-1 in adult male germlines in parallel with adult hermaphrodite

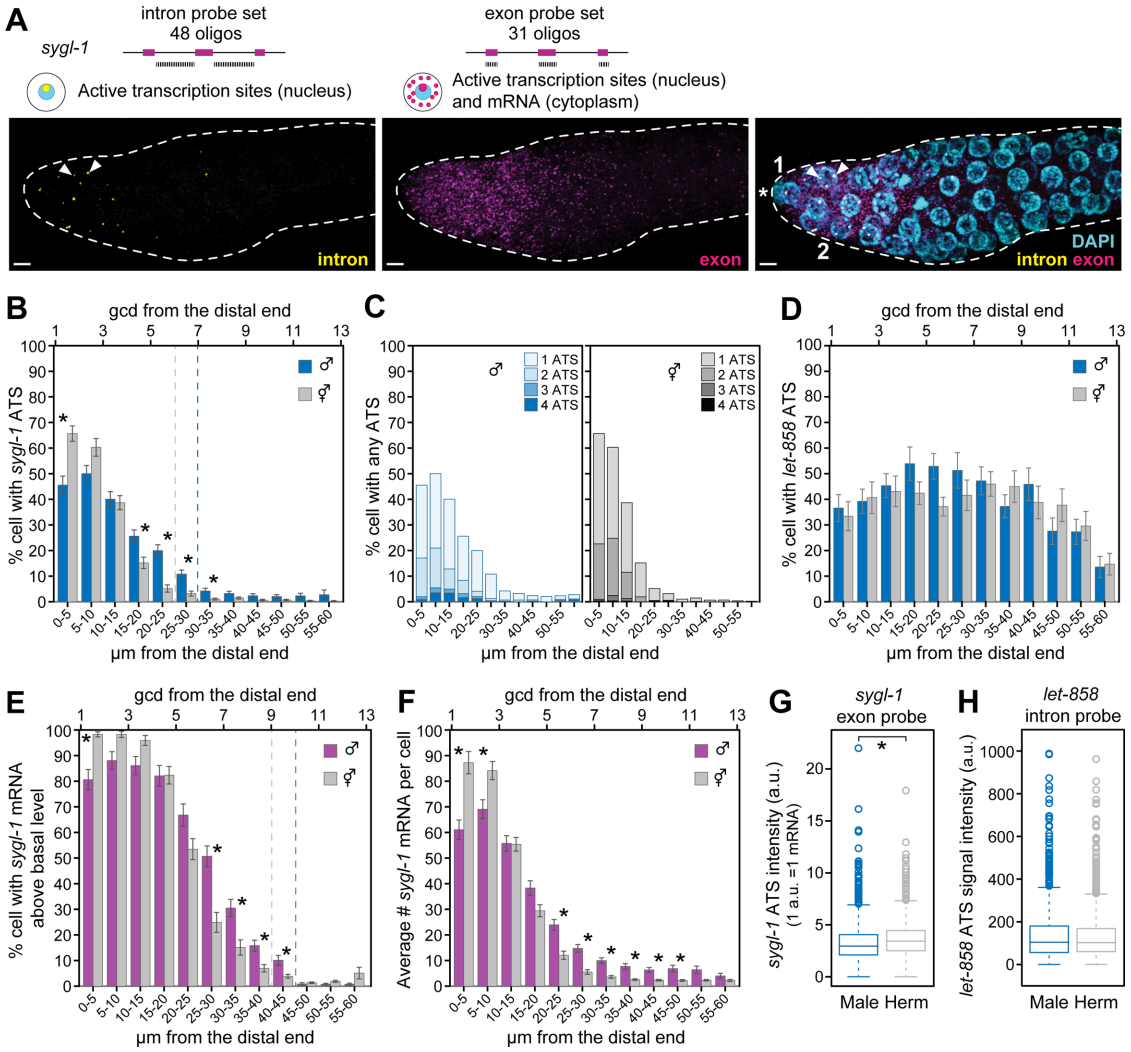

FIGURE 4: GLP-1/Notch-dependent transcription in mPZ. Single molecule FISH (smFISH) detects GLP-1/Notch-dependent transcription from the *sygl-1* locus, as done previously in hermaphrodites (Lee *et al.*, 2016). (A) Representative images of the distal end of a male gonad showing signals from the intron probe (left), exon probe (middle), and merge of both intron and exon probes with DAPI (right). smFISH probes and expected subcellular distributions for exon and intron probes are diagrammed above the images. Positions of DTC nuclei are marked 1 and 2 in the merged panel. Two ATS are marked with white arrowheads in the intron and merged panels. (B, C, E–G) Quantitation of *sygl-1* smFISH signals in male and hermaphrodite gonads processed in parallel for this work. Males $n = 60$, hermaphrodites $n = 49$. Error bars: SE of the mean. *Statistical significance of $p < 0.01$. (B) The percentage of cells with ATS. Male (blue bars) and hermaphrodite (gray bars). Dotted lines mark positions in males (blue) and hermaphrodites (gray) where the percentage of cells with ATS drops below 5%. ATS were restricted to a region of 1–30 µm (~1–7 gcd) in males and 1–25 µm (~1–6 gcd) in hermaphrodites. (C) Same data as in B showing the percentage of cells with 1, 2, 3, or 4 ATS per nucleus indicated. Distal germ cells are more likely to have more than one ATS than more proximal cells. (D) Quantitation of control *let-858* ATS detected with *let-858*–specific intron probes. Males $n = 24$, hermaphrodites $n = 20$. The percentage of cells with *let-858* ATS is not graded and is not significantly different between males and hermaphrodites. The *p* values are all greater than 0.01. (E) The percentage of cells with mRNA above basal level (see *Materials and Methods* for basal level calculation). Male (magenta bars) and hermaphrodite (gray bars). Dashed lines mark positions in males (magenta) and hermaphrodites (gray) where the percentage of cells drops below 5%. The percentage of cells with mRNA is higher in proximal rows than the percentage of cells with ATS in both sexes (compare B and E). (F) The number of mRNA/cell in males (magenta) and hermaphrodites (gray). (G) Signal intensity of *sygl-1* ATS in male (left) and hermaphrodite (right). Intensity units are the average intensity of a single mRNA (a single mRNA = 1 a.u.; see *Materials and Methods*). The mean for males is 3.3; for hermaphrodites, it is 3.6. The signal intensity is significantly different between males and hermaphrodites ($p < 0.01$); however, the difference is less than the intensity of a single mRNA. (H) Signal intensity of *let-858* ATS in male (left) and hermaphrodite (right). This value is calculated using signals from intron probes, which is different from that in G, which used exon probes. They are not significantly different ($p = 0.43$).

germlines. SYGL-1 and LST-1 protein expression is high in the distal PZ in male germlines (Figure 6, A and B), a pattern similar to that reported previously for hermaphrodites (Shin, Haupt, *et al.*, 2017). Moreover, SYGL-1 was largely cytoplasmic (Figure 6A), while LST-1 was strikingly associated with perinuclear granules as well as being cytoplasmic (Figure 6B), similar to hermaphrodites

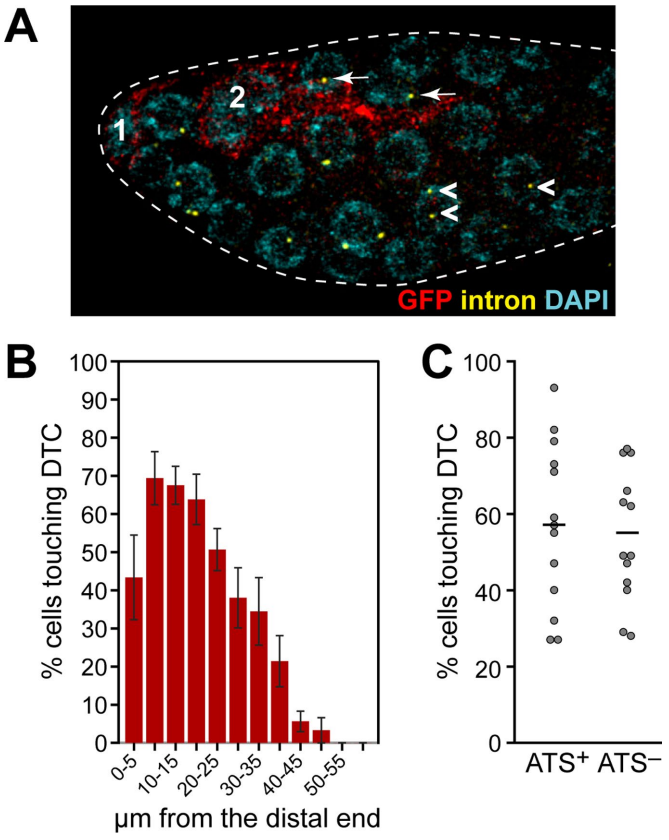

FIGURE 5: Male DTCs and their association with *sygl-1* ATS-positive germ cells. (A–C) The *sygl-1* smFISH was done on animals carrying the P*arg-1*::myrGFP transgene. GFP reveals mDTC (red) and intron probe reveals ATS (yellow). (A) This image of a male gonad shows cells with ATS both with (white arrows) and without (white arrowheads) detectable contact with the mDTCs. (B, C) MATLAB quantitation of male ($n = 13$) gonads. (B) The percentage of germ cells with detectable DTC contact in distal-most 60 µm of germline in males. (C) The percentage of ATS-positive and ATS-negative germ cells with detectable DTC contact in the distal 1–13 gcd (60 µm) of male germlines. The percentages varied from gonad to gonad. Means (black bars): ATS-positive 57%, ATS-negative 54%.

(Shin, Haupt, *et al.*, 2017). Remarkably, the levels of SYGL-1 and LST-1 expression and their extents were similar in males and hermaphrodites (Figure 6B), and the number of germ cells expressing each protein was also similar in the two sexes (Figure 6C). In both sexes, SYGL-1 and LST-1 levels are high in the distal rows of the GSC pool; LST-1 decreases within the pool and SYGL-1 decreases near the proximal boundary of the pool.

In addition to distal germline expression, we examined proximal germline expression (Figure 7). In males, *sygl-1* RNA was absent from the proximal germline (Figure 7A, left), which contrasts with the previously reported *sygl-1* expression in the proximal hermaphrodite germline (Figure 7A, right) (Lee *et al.*, 2016). Similarly, SYGL-1 protein was not detectable in the proximal male germline (Figure 7B, left) but was abundant in the proximal hermaphrodite germline (Figure 7B, right), as previously reported (Shin, Haupt, *et al.*, 2017). The LST-1 pattern was opposite: abundant in the male proximal germline (Figure 7C) but faint in the hermaphrodite proximal germline (Figure 7C, right) (Shin, Haupt, *et al.*, 2017). This proximal LST-1 was predominantly cytoplasmic (Figure 7C, inset). Thus, SYGL-1 and LST-1 expression is similar in the distal germlines of the two sexes, but distinct in their proximal germlines.

DISCUSSION

This study investigates how sexual dimorphism of the niche for GSCs in *C. elegans* affects the size of the stem cell pool and shape of the GSC response to niche signaling. Briefly, GSC pool size and the molecular response to signaling are remarkably similar in the two sexes despite differences in niche architecture (Figure 8). Below we discuss our results and put them into broader context.

GSC pool size is comparable in males and hermaphrodites

Previous studies identified the hermaphrodite GSC pool, which extends roughly 6–8 gcd from the distal end and contains 30–70 germ cells (Cinquin, Crittenden, *et al.*, 2010; Shin, Haupt, *et al.*, 2017). The 30–70 estimate of cell number embraces counts in the *emb-30* assay (~30) as well as counts of the equivalent region in wild type (~50–70). Here we identify the male GSC pool and find its size similar to that of hermaphrodites. Given differences in mDTC architecture and male germline characteristics (see *Introduction*; e.g., folds, cell cycle rate), we expected a male-specific size, but the male GSC pool also extends roughly 6–8 gcd from the distal end and also contains 30–50 germ cells. Therefore, both the extent and cell number are comparable in the two sexes despite striking differences in niche architecture (Figure 8, A and C) (Cinquin, Crittenden, *et al.*, 2010; Shin, Haupt, *et al.*, 2017; this work).

Extent of niche contacts with germ cells is sexually dimorphic

The positions of DTC cell bodies have been known for decades (Kimble and White, 1981; Morgan *et al.*, 2010), but mapping DTC cytoplasmic processes has been recent and facilitated by the use of myristoylated GFP. The hDTC generates an extensive plexus of processes that contact essentially all germ cells in the GSC pool (Byrd *et al.*, 2014; Lee *et al.*, 2016), and we predicted that mDTCs might generate a similar plexus to provide similarly extensive contacts with cells in the GSC pool. However, this is not the case. Male DTCs do not form a plexus and contacts with cells in the GSC pool were much less extensive in males than in hermaphrodites (Figures 5 and 8, A and B). This finding raises a question about the role of the hDTC plexus in GSC regulation. In hermaphrodites, the DTC plexus does not exist in larval hermaphrodites though GSCs are maintained. The absence of a plexus in adult males reinforces the notion that extensive niche contact is not necessary for the maintenance of a stem cell pool. The DTC cell body or cap is common to various stages of development and both sexes, and in each case, the cap covers germ cells and inserts short intercalating processes between them (Byrd *et al.*, 2014; Linden *et al.*, 2017; Pekar *et al.*, 2017). The cap is therefore sufficient for effective niche signaling and may be the primary source. This intimate interaction of niche with stem cells is shared in other stem cell systems (Tamplin, Durand, *et al.*, 2015; Franca *et al.*, 2016; Spéder and Brand, 2018) and can be induced by stem cells themselves (Tamplin, Durand, *et al.*, 2015; Gordon, Payne, *et al.*, 2019). We suggest that the plexus may reinforce cap signaling or serve a different purpose (e.g., anchoring or protecting GSCs [Song *et al.*, 2002; Bailey *et al.*, 2015; Kapp *et al.*, 2018]).

Transcriptional activation in response to niche signaling occurs in the absence of niche contact

Notch-dependent ATS, visualized using smFISH, provide a direct readout of active Notch signaling (Lee *et al.*, 2016). Hermaphrodite *sygl-1* ATS occur across a region corresponding to the GSC pool, with virtually all cells bearing *sygl-1* ATS touching the hDTC cap or plexus. The correlation between Notch-dependent transcriptional activation and niche contact is thus high in adult hermaphrodites.

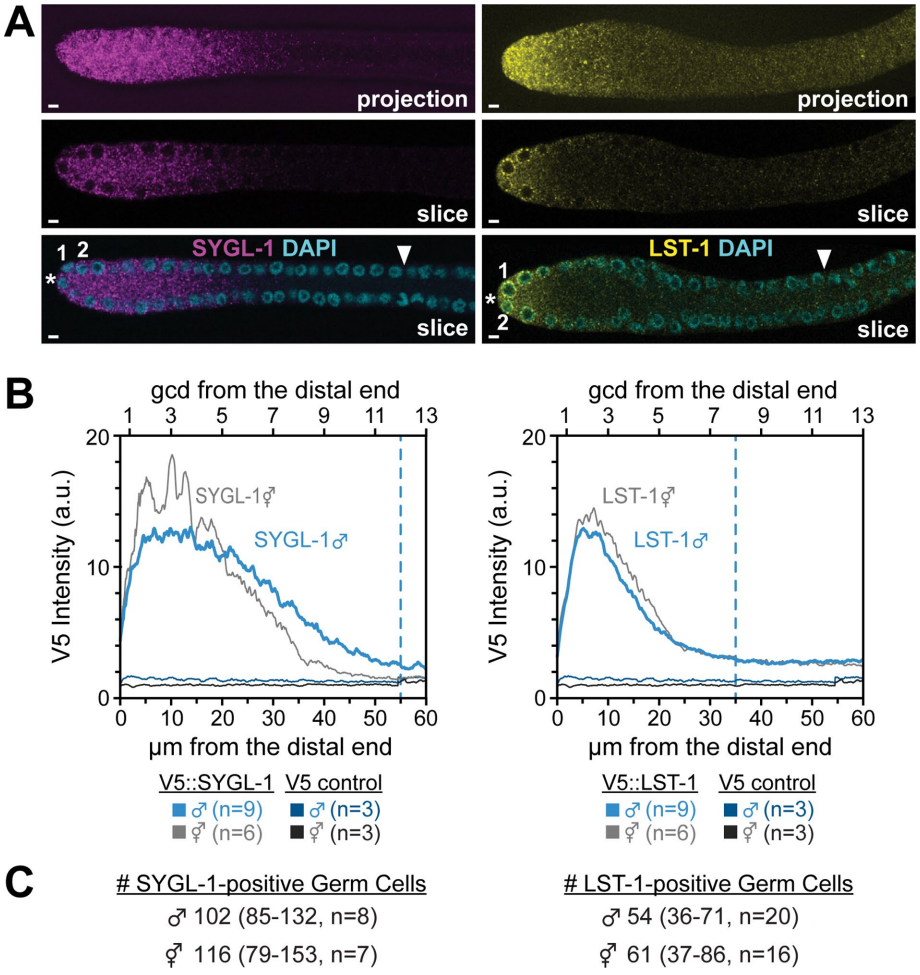

FIGURE 6: Expression of key stem cell regulators, SYGL-1 and LST-1, in the distal gonad. SYGL-1 and LST-1 proteins were V5-tagged and visualized with a V5 antibody, as reported previously for hermaphrodites (Shin, Haupt, *et al.*, 2017). (A) Immunostaining of male distal gonads: SYGL-1 (magenta, left panels) and LST-1 (yellow, right panels). Top panels: single channel maximum intensity confocal projections. Middle panels: single channel, single confocal slice through the middle of gonad. Bottom panels: same as the middle panel, merged with DAPI. *Distal end. (B) ImageJ quantitation of z projections of stained gonads, all done in parallel. Expression in males (blue); expression in hermaphrodites (gray) ($n = 9$ for both SYGL-1 and LST-1 males; $n = 6$ for both SYGL-1 and LST-1 hermaphrodites; $n = 3$ for both control males and hermaphrodites). Dashed lines indicate the average position where expression dropped to a background level when scored by eye. (C) Number of germ cells positive for LST-1 or SYGL-1 in male or hermaphrodite germlines.

However, this is not the case in adult males (Figures 4 and 8, D and E). Asymmetric mDTC localization and lack of a plexus leaves many germ cells without niche contact, but male *sygl-1* ATS are generated in a region similar to that of hermaphrodites, including regions with little or no mDTC contact. The response to GLP-1/Notch signaling is therefore similar in the two sexes despite the dimorphism in niche architecture. Understanding how variable niche architecture affects stem cell regulation has implications for tissues where the niche changes its size or morphology in response to changing conditions (Boyle, Wong, *et al.*, 2007; Degirmenci, Valenta, *et al.*, 2018; Shoshkes-Carmel *et al.*, 2018).

The *sygl-1* transcriptional activation in germ cells lacking niche contact presents an intriguing paradox. Canonical Notch signaling relies on the interaction between a membrane-bound Notch ligand on the signaling cell and a membrane-bound Notch receptor on the adjacent receiving cell; ligand endocytosis exerts a pulling force on the Notch receptor to trigger receptor cleavage, nuclear entry of the released intracellular domain, and Notch-dependent transcriptional activation (Kovall *et al.*, 2017; Luca *et al.*, 2017). How might *sygl-1* transcription be activated in germ cells lacking niche contact? Answering this question remains a challenge for the future, but we suggest a few possible explanations. First, our snapshot images may not have detected all mDTC processes and their germ cell contacts because they are dynamic, difficult to fix, and/or difficult to image, similar to cytonemes (Wong, Paz, *et al.*, 2013; Huang and Kornberg, 2015). Second, a diffusible Notch ligand may be involved. The *C. elegans* genome encodes several Notch ligands predicted to lack a transmembrane domain (Chen and Greenwald, 2004; Komatsu *et al.*, 2008). One such ligand, DSL-1, affects Notch-mediated patterning of the vulva (Chen and Greenwald, 2004) and PZ size in the male germline (this work; Table 1). A third possibility is that regulators generated downstream of the ligand-receptor interaction are able to diffuse between cells in the germline syncytium and thus extend the response beyond the region of niche contact. The male germline is thus poised to expand our understanding of how Notch signaling can pattern a tissue.

GLP-1/Notch signaling and patterning the GSC pool

Germ cells in the GSC pool are equivalent in having similar cell cycle rates (Crittenden *et al.*, 2006; Morgan *et al.*, 2010) and failing to differentiate upon cell cycle arrest (Cinquin, Crittenden, *et al.*, 2010; Fox *et al.*, 2011; Jeong *et al.*, 2011; this work) (Figure 3). However, molecular and cellular differences among cells in the GSC pool have emerged. Three differences have been seen in both sexes. First, the transcriptional response to GLP-1/Notch signaling is highest in the distal 1–3 gcd and steeply graded more proximally (this paper; Lee *et al.*, 2016) (Figure 8, D and E). Second, SYGL-1 protein is present throughout the pool, but LST-1 is restricted to the distal-most 4–5 rows (Shin, Haupt, *et al.*, 2017) (Figure 8F). Third, cells in the distal 1–3 rows have extensive contact with the DTC cap (this paper; Byrd *et al.*, 2014; Linden *et al.*, 2017) (Figure 8, A and B). Other differences have been seen in hermaphrodites but have not been tested in males. Thus, germ cells in the distal-most 1–2 rows have subtly distinct cell cycle characteristics (Crittenden *et al.*, 2006; Maciejowski *et al.*, 2006) and remain in place at the distal end, while more proximal germ cells move out of the GSC pool and eventually differentiate (Rosu and Cohen-Fix, 2017). In summary, the distal-most ~10 germ cells are distinguished by having extensive contact with the DTC cap, the highest response to GLP-1/Notch signaling and the highest levels of LST-1 and SYGL-1. These shared characteristics are consistent with a model that the

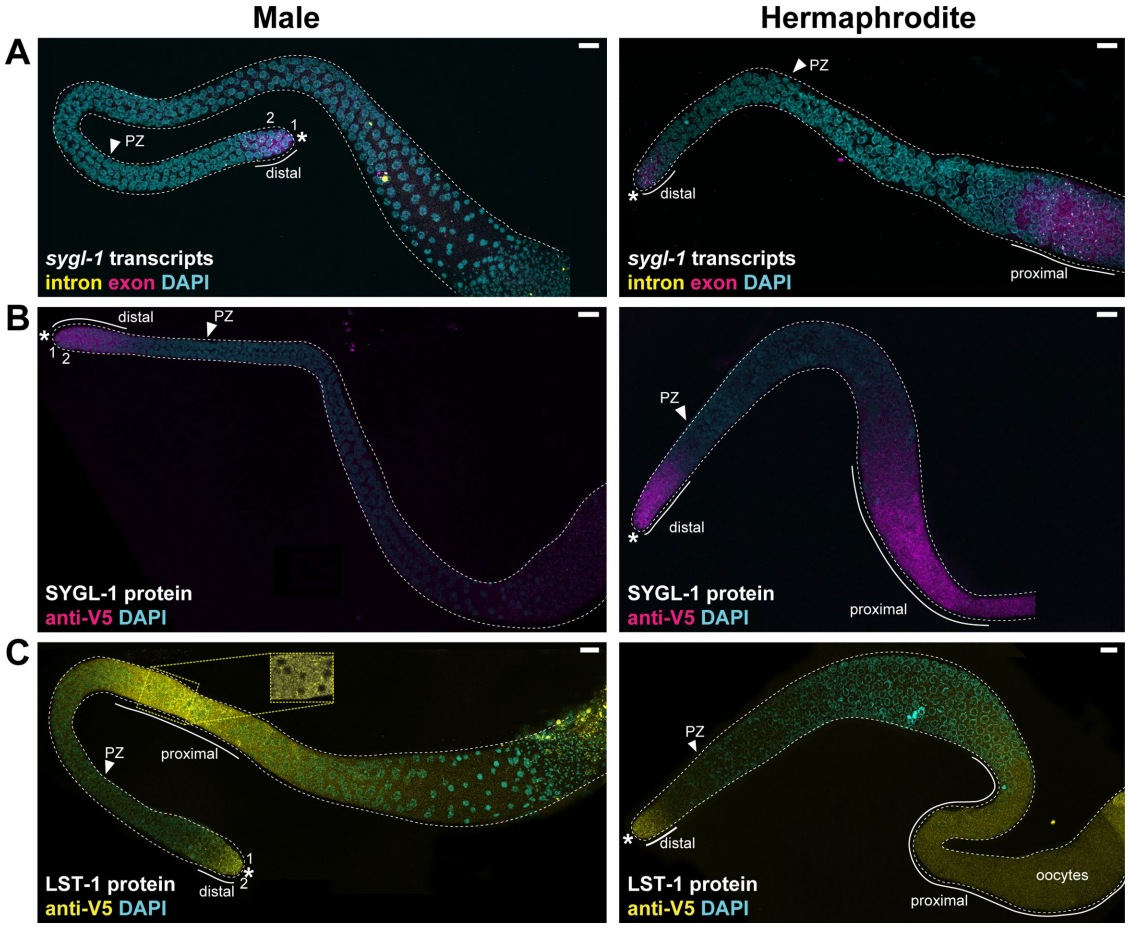

FIGURE 7: The *sygl-1* and *lst-1* mRNA and protein expression in whole gonads. (A–C) Projected confocal z stacks of adult male (left) or hermaphrodite (right) entire gonads. An asterisk marks the distal end; PZ arrowhead marks proximal boundary of the PZ. (A) The *sygl-1* smFISH. The *sygl-1* transcripts are limited to the distal end of male gonads (this work), but in hermaphrodites, they are found both distally and proximally, as reported before (Kershner *et al.*, 2014; Lee *et al.*, 2016). (B) SYGL-1 immunostaining. SYGL-1 protein is limited to the distal end of male gonads (this work), but in hermaphrodites, SYGL-1 is found both distally and again proximally, as reported before (Shin, Haupt, *et al.*, 2017). (C) LST-1 immunostaining. Male germlines express LST-1 protein in a restricted region in the distal germline and also more proximally. LST-1 is enriched in perinuclear granules distally (Figure 6A), but is less granular proximally (inset). Inset is taken from a single confocal slice in the area indicated by the yellow dotted box in the full germline image. In hermaphrodites, LST-1 expression is strong distally and weak proximally, as reported before (Shin, Haupt, *et al.*, 2017). *Distal end.

distal-most germ cells in the pool continuously self-renew, while more proximal cells in the GSC pool have the potential for self-renewal but ultimately differentiate. Stem cell progeny that retain the potential to become stem cells, although they normally differentiate, also occur in fly and mouse germlines (Spradling *et al.*, 2011) as well as in several vertebrate somatic tissues (e.g., Visvader and Clevers, 2016). A challenge for the future is to address the interplay of varied tissue architectures with the regulatory networks that control stem cells.

MATERIALS AND METHODS

Strains and worm maintenance

C. elegans animals were maintained by standard techniques and grown at 20°C unless otherwise noted. Strains used were: N2, DG627 *emb-30(tn377ts)* (Furuta *et al.*, 2000), PD4443 *ccIs4443[Parg-1::GFP + dpy-20(+)] IV* (Kostas and Fire, 2002), JK5764 *qSi361[Parg-1::myrGFP::tbb-2] IV* (this work), JK5929 *lst-1(q1004) I* (Shin, Haupt, *et al.*, 2017), JK6002 *sygl-1(q1015) I* (Shin, Haupt, *et al.*, 2017), EG8081 *unc-119(ed3) III; oxTi177 IV* (Frøkjær-Jensen *et al.*, 2014), JK4475 *qIs153[Plag-2::myrGFP] III*, JK4533 *qIs153[Plag-2::myrGFP] III* outcrossed, JK4542 *qIs153 III/ eT1[qIs60](III;V); lag-2(q411) V/ eT1[qIs60](III;V)*, JK4511 *qIs153 III; apx-1(or3)/ DnT1(IV;V)*, JK4540 *qIs153 III/ eT1[qIs60](III;V); apx-1(or3) V/ eT1[qIs60](III;V)*, JK4509 *qIs153 III; arg-1(ok3127) X*, JK4507 *qIs153 III; dsl-1(ok810) IV*, JK4546 *qIs153 III; dsl-4(ok1020) X*, JK4538 *qIs153 III/ eT1[qIs60](III;V); lag-2(q411) V/ eT1[qIs60](III;V); arg-1(ok3127) X*, JK4541 *qIs153 III/ eT1[qIs60](III;V); dsl-1(ok810) IV; lag-2(q411) V/ eT1[qIs60](III;V)*, JK4539 *qIs153 III/ eT1[qIs60](III;V); apx-1(or3) V/ eT1[qIs60](III;V); arg-1(ok3127) X*.

Transgenes used to visualize male DTC architecture

For male DTC architecture, we used strains containing P*arg-1*::GFP (PD4443: *ccIs4443 IV* (Kostas and Fire, 2002) or P*arg-1*::myrGFP (JK5764: *qSi361 IV*). P*arg-1*::myr GFP is a Mos insertion of plasmid pJK2010 into the Mos insertion site *oxTi177 IV*. pJK2010 was created using Gibson assembly of 6.1 kb of genomic DNA upstream of the *arg-1* start site, myristoylated GFP from plasmid pJK1709, and the Mos insertion plasmid pCFJ151 (Frøkjær-Jensen *et al.*, 2014).

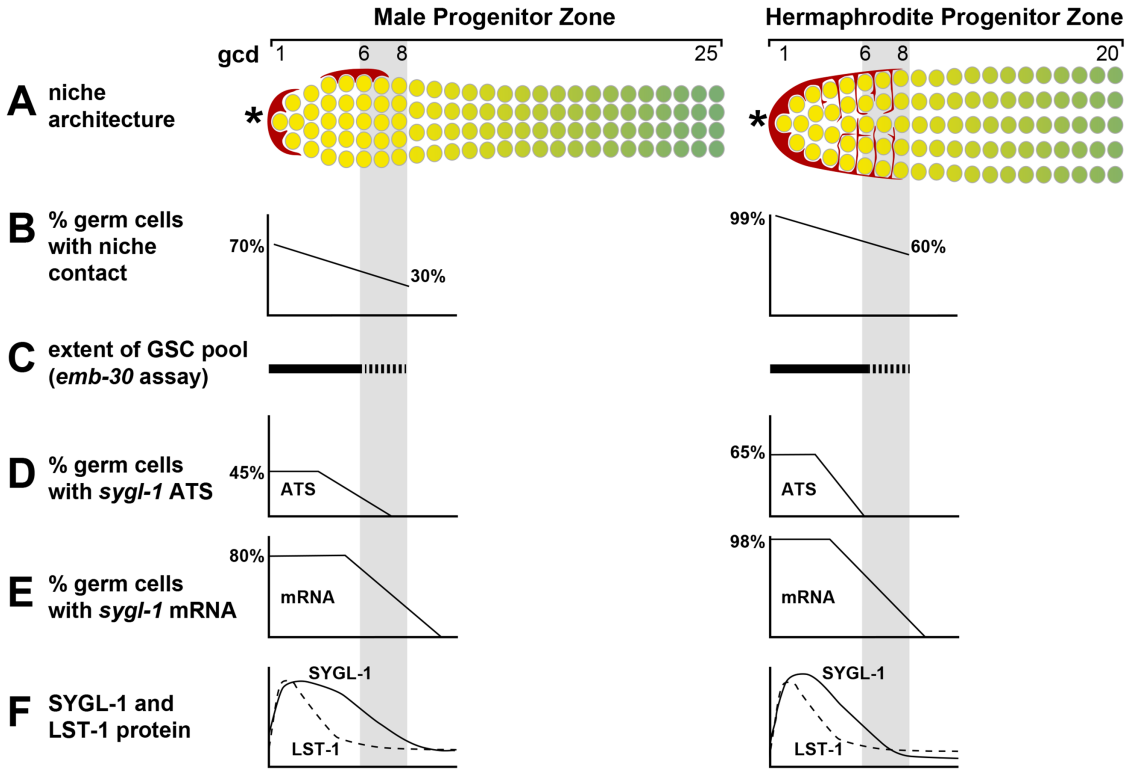

FIGURE 8: Summary of niche and PZ features in males and hermaphrodites. Gray shading marks the estimated boundary of the GSC pool (range 6–8 gcd in both sexes). (A) Diagrams of niche architecture and PZ extent. Left, males possess two asymmetrically positioned mDTC cell bodies or caps that extend minimal cytoplasmic processes and do not form a plexus; right, hermaphrodites possess a single DTC that extends elaborate cytoplasmic processes that form a plexus (red lines between GSCs). *Distal end. (B–F) Graphs summarizing key features. (B) Niche contacts are fewer in males than in hermaphrodites. (C) GSC pool extents are equivalent in the two sexes. (D) The percentage of cells with *sygl-1* ATS is lower in the distal germ cells in males but higher more proximally than in hermaphrodites. (E) The percentage of cells with *sygl-1* mRNAs is also lower in distal germ cells in males but higher more proximally than in hermaphrodites. (F) SYGL-1 protein extends slightly more proximally in males than in hermaphrodites but LST-1 extents are indistinguishable.

The expression pattern was similar for both PD4443 and JK5764 transgenes, but GFP was membrane-associated with JK5764, as expected, and expression was low with JK5764, consistent with a single copy insertion. Animals were scored both live and fixed with similar results. Live animals were staged, mounted on agarose pads with either levamisole or 0.1 µm Polybeads (Polysciences) or both, and imaged on either a Zeiss LSM510 or a Leica SP8 confocal microscope.

Scoring DSL ligand mutant PZs

Adult males, 24 h after L4, were dissected and gonads extruded into 0.25 mM levamisole in M9 containing Hoechst 33342 (Invitrogen) at 100 ng/ml. PZ was scored as described (Crittenden *et al.*, 2006). Briefly, the PZ extends from the distal-most germ cell to the start of early meiotic prophase, defined as the position where more than one germ cell has crescent-shaped DNA staining typical of early leptotene/zygotene.

emb-30 assay

The *emb-30* cell cycle arrest assay was done as described previously (Cinquin, Crittenden, *et al.*, 2010). The *emb-30(ts)* animals were grown at permissive temperature (15°C) until 36 h past L4 and then shifted to restrictive temperature (25°C). Gonads were dissected, fixed, and stained with anti-PH3, anti-GLD-1, and/or DAPI after specified time intervals. We note that M-phase arrest was more variable in males than hermaphrodites. To estimate the cell number in the distal GSC pool, we counted the number of M–phase-arrested cells distal to the high GLD-1 boundary using the multipoint tool in FIJI (Schindelin *et al.*, 2012). This number is likely an underestimate since *emb-30* mutants have a slightly smaller PZ than wild type even at permissive temperature (Furuta *et al.*, 2000). We excluded gonads in which the majority of GSC pool nuclei were fragmented because they could not be reliably counted (3/10 hermaphrodites and 7/15 males).

Immunohistochemistry

Males and hermaphrodites containing V5-tagged LST-1 or SYGL-1 or P*arg-1*::myrGFP were picked as mid-L4s and gonads were dissected 22–26 h later (A24 adults). Gonads were extruded, fixed, and stained using standard protocols (Crittenden *et al.*, 2017). Animals were washed off plates in ~200 µl phosphate-buffered saline (PBS) containing 0.1% Tween 20 (PBSTw) and 0.25 mM levamisole and pipetted into a multiwell dish. They were then cut behind the pharynx to extrude the gonad and pipetted into a 1.5-ml microfuge tube, and 4% paraformaldehyde was added for 10 min at room temperature. After centrifugation at 1500 rpm for 30 s, excess liquid was removed and gonads were permeabilized with 100 µl PBSTw containing 0.5% bovine serum albumin (PBSBTw) and 0.5% Triton X-100 for 5 min at room temperature. Centrifugation was repeated and gonads were blocked in PBSBTw for 30 min at room temperature. Primary antibodies were

added and tubes were placed at 4°C overnight. Mouse anti-V5 (Bio-Rad) was used at 1:1000–1:5000; mouse anti-GFP (3E6, Invitrogen) was used at 1:200. Secondary antibodies (Alexa 488, Alexa 555, and Alexa 647; Jackson ImmunoResearch) were used at 1:1000 in PBSBTw containing 1 µg/ml DAPI and incubated for 1 h at room temperature on a rotating rack shielded from light, followed by three washes in PBSBTw. Finally, samples were mounted in 10 µl ProLong Gold (ThermoFisher) and covered with a 22 × 22 coverslip, allowed to cure overnight to several days, and imaged on a Leica SP8 confocal microscope.

Imaging and quantitating *sygl-1* transcripts

We used the previously described smFISH protocol, imaging parameters, and quantitation and analysis tools with modifications (Lee *et al.*, 2016, 2017). Males and hermaphrodites, 24 h after mid-L4, were dissected in ~200 µl PBS, 0.1% Tween 20 (PBSTw) containing 0.1% tricaine and 0.01% tetramisole. Dissected worms were pelleted at 1500 rpm for 30 s, fixed in 1 ml PBSTw, 3.7% formaldehyde, pelleted, washed in PBSTw, and permeabilized in PBS containing 0.1% Triton X-100 for 10 min at room temperature. Samples were washed two times and resuspended in 1 ml 70% ethanol and stored at 4°C overnight or up to 1 wk. Samples were washed and hybridized with probes (*sygl-1* intron, 48 unique oligonucleotides, QUASAR 570; *sygl-1* exon, 31 unique oligonucleotides, CALFLUOR 610; and/or *let-858* intron, 48 unique oligonucleotides, CALFLUOR 610; Biosearch Technologies) overnight at 37°C, protected from light. Following hybridization, samples were washed at room temperature, incubated with 1 ml wash buffer containing 1 µg/ml DAPI for 30 min, washed two additional times, and then mounted in ProLong Gold and allowed to cure overnight to several days before imaging. Images were acquired using a Leica SP8 confocal microscope essentially as described (Lee *et al.*, 2016).

The *let-858* ATS analysis (Figure 4D) used only one smFISH probe set targeting the intronic regions of *let-858*, unlike *sygl-1* analyses where two sets of (intron- or exon-specific) probes were used. The *let-858* ATS were identified and scored the same way as in *sygl-1* analyses but without exon channel cross-validation. The *let-858* ATS intensity was measured using intron probe only, while *sygl-1* intensity was measured using the exon probe so that it could be normalized to mRNA intensity.

The mRNA basal level was calculated using the 97.5th percentile of the rare cytoplasmic signals outside the distal GSC pool region, between 45 and 65 µm or ~10–14 gcd from the distal end in each gonad. For each gonadal image, the percentage of cells with mRNA was calculated using the basal level from the same gonad (Figure 4E). The *p* values for smFISH were calculated using two-sample *t* test unless otherwise noted. For all box-and-whisker plots in this study, the bold line in the box shows the median; the top and bottom of the box are the third and first quartiles, respectively; whiskers, maximum and minimum of data points; circles, outliers (value greater than 1.5× first or third quartile from the median). For all analyses, we excluded gonadal images for each sex that had a greater than fivefold increase (2/60 for males and 2/53 for hermaphrodites) or a greater than fivefold decrease (2/60 for males and 2/53 for hermaphrodites) in the average total number of mRNAs per gonad.

MATLAB code modifications

Quantitation was done with modified custom MATLAB codes (v1.03; https://github.com/chlasic/smFISH_detection_analysis). The codes were significantly improved in efficiency and accuracy since their initial publication (Lee *et al.*, 2016). In addition, some modular MATLAB functions have been rewritten to implement more rigorous and precise algorithms. While ATS and mRNA analyses in the hermaphrodite gonad are similar using the 2019 code reported in this work and the code used in Lee *et al.* (2016), the results from each of the two versions of the code varied in the following two ways: 1) estimation of number of transcripts at the ATS by comparison to mean mRNA intensity (Figure 4G) and 2) estimation of number of mRNA per germ cell (Figure 4F). We reanalyzed images from Lee *et al.* (2016) ($n = 78$ adult hermaphrodite gonads) with the updated 2019 code and the results were essentially the same as the current study. Manual counting and quantitation in ImageJ ($n = 3$ gonads) confirmed the results from the new code.

Three MATLAB functions from the previously published smFISH detection code v18 (Lee *et al.*, 2016, 2017) were modified in the current version, v1.03 (this paper): 1) the DetectRNAintron function was improved to reduce false-positive and false-negative spots and to allow detection of dimmer and smaller ATS spots. Briefly, parameters in functions for spot detection (Gaussian fitting, image segmentation, and local peak detection) were optimized using a larger training set (50 random images as opposed to 15 images in the previous version). A new algorithm (local signal-to-noise measurement) was implemented and applied for three iterations, each with a different scanning window size (two, three, and four times the detected spot size in each iteration). ATS candidates with signal-to-noise ratio less than 1.5 are removed in each iteration. 2) The DetectRNAexon function was modified to improve detection of individual mRNA spots. Several mRNAs in close proximity could have been detected as a single mRNA spot with the previous MATLAB code. This could skew the mean intensity of a single mRNA as well as the estimation of the number of transcripts per ATS. The new code uses a 2× smaller scanning disk during image segmentation, resulting in a ~1.5- to 2-fold increase in the count for overall mRNA in a gonad. These new counts were verified by manual counting ($n = 3$ gonads). Estimation of the number of transcripts per ATS changed substantially using the current code. This is because the current code uses the exon signal at an ATS directly (after cross-validation with intron probe), while the previous code recorded only the intron signals and then used the mean ratio of intron/exon signal to back calculate exon signal at an ATS. 3) The MatchrnaNuc function was improved by reducing the size of the binary mask (2× smaller threshold value for imdilate function) to improve nuclear detection.

We also made several additional improvements. Background signal is measured specifically inside the gonad. The previous version of the code used all regions in the field of view instead. Gonad boundaries are identified using the low background signal present throughout the gonad in the intron channel (3–7 a.u./pixel), which is higher than regions outside of the gonad (0–1 a.u./pixel). Masks of the gonad were generated using image segmentation. The previous MATLAB code identified ATS candidates using only the intron signal followed by recording the integrated exon signal in the same region where ATS was detected. If the exon signal at a given ATS candidate met the criteria (signal-to-noise ratio >1.9 [to overall background] and >1.27 [to local background], *p* value of signal and noise $<9{\cdot}10^{10}$), the ATS was considered a true ATS (Lee *et al.*, 2016). With the current MATLAB code, ATS candidates are independently detected in exon and intron channels, and candidates are cross-validated between the channels to identify true ATS. In addition, the current code improves representation of the nucleus. Instead of creating DAPI masks using the MATLAB function imbinarize as in the previous code, we used the imfill function to fill small gaps in DAPI staining to reconstruct a spherical nuclear mask. We found that this new mask better represented the nucleus and had better results for ATS subcellular localization compared with manual counting ($n = 10$ gonads).

Detection and quantitation of DTC contact with germ cells

Gonads from JK5764 (P*arg-1*::myrGFP) males and hermaphrodites 24 h after L4 were fixed and hybridized with *sygl-1* intron probes as described above, except that gonads were mounted in ProLong Glass, cured overnight, and then either imaged or stored at –20°C. Images of smFISH and GFP signals were acquired with a Leica SP8 resonance scanner and deconvolved using Leica Lightning. Images were analyzed using customized MATLAB codes (Lee *et al.*, 2016) with minor modifications. Briefly, a binary image of GFP signal (DTC mask) was created on each z-plane. The signal intensity of each pixel was considered significant if it was more than four times brighter than the overall mean background intensity in the corresponding z-plane of the gonad. Individual binary z-plane images from each gonad were combined and reconstructed in three dimensions and overlaid with DAPI. Boundaries between germ cells were estimated using Voronoi segmentation as described in Lee *et al.* (2016) using 3 μm as maximum cell radius. Germ cell boundaries with more than 10 pixels of GFP signal above background level were scored as DTC-contact-positive. *sygl-1* ATS were also scored in the same gonads. By eye, we confirmed the existence of ATS-positive nuclei that were separated from detectable DTC GFP by at least one germ cell nucleus in all dimensions; an example of this is shown in Figure 5A (arrowheads).

Imaging and quantitating LST-1 and SYGL-1 protein

LST-1:V5 and SYGL-1:V5 proteins were imaged as previously described (Shin, Haupt, *et al.*, 2017). Protein levels were quantitated in summed projections of confocal stacks using ImageJ. Briefly, a line (linewidth = 50 pixels) was drawn along the distal-proximal axis of the germline. Pixel intensity was measured using the plot profile function. Intensities were copied into MATLAB, averaged, and graphed. An N2 wild-type control was used to quantitate background for anti-V5.

ACKNOWLEDGMENTS

We thank Brandon Taylor for the P*arg-1*::myr GFP plasmid and discussions, Dana Byrd for preliminary observation of P*arg*-1::GFP in male DTCs, Laura Vanderploeg for help with figures, Tina Lynch and Kim Haupt for comments on the manuscript, and Anne Helsley-Marchbanks for assistance with manuscript preparation. Funding was provided by the National Institutes of Health (GM-069454 to J.K.) as well as the Stem Cell and Regenerative Medicine Center within the University of Wisconsin School of Medicine and Public Health. J.K. is an investigator of the Howard Hughes Medical Institute. Some strains were provided by the Caenorhabditis Genetics Center, which is funded by the National Institutes of Health Office of Research Infrastructure Programs (P40 OD010440).

REFERENCES

Boldface names denote co–first authors.

Amini R, Goupil E, Labella S, Zetka M, Maddox AS, Labbe JC, Chartier NT (2014). *C. elegans* anillin proteins regulate intercellular bridge stability and germline syncytial organization. J Cell Biol 206, 129–143.

Austin J, Kimble J (1987). *glp-1* is required in the germ line for regulation of the decision between mitosis and meiosis in C. elegans. Cell 51, 589–599.

Bailey AP, Koster G, Guillermier C, Hirst EM, MacRae JI, Lechene CP, Postle AD, Gould AP (2015). Antioxidant role for lipid droplets in a stem cell niche of *Drosophila*. Cell 163, 340–353.

Boyle M, Wong C, Rocha M, Jones DL (2007). Decline in self-renewal factors contributes to aging of the stem cell niche in the *Drosophila* testis. Cell Stem Cell 1, 470–478.

Brenner JL, Schedl T (2016). Germline stem cell differentiation entails regional control of cell fate regulator GLD-1 in *Caenorhabditis elegans*. Genetics 202, 1085–1103.

Byrd DT, Knobel K, Affeldt K, Crittenden SL, Kimble J (2014). A DTC niche plexus surrounds the germline stem cell pool in *Caenorhabditis elegans*. PLoS One 9, e88372.

Chen N, Greenwald I (2004). The lateral signal for LIN-12/Notch in *C. elegans* vulval development comprises redundant secreted and transmembrane DSL proteins. Dev Cell 6, 183–192.

Cinquin O, Crittenden SL, Morgan DE, Kimble J (2010). Progression from a stem cell-like state to early differentiation in the *C. elegans* germ line. Proc Natl Acad Sci USA 107, 2048–2053.

Crittenden SL, Bernstein DS, Bachorik JL, Thompson BE, Gallegos M, Petcherski AG, Moulder G, Barstead R, Wickens M, Kimble J (2002). A conserved RNA-binding protein controls germline stem cells in *Caenorhabditis elegans*. Nature 417, 660–663.

Crittenden SL, Leonhard KA, Byrd DT, Kimble J (2006). Cellular analyses of the mitotic region in the *Caenorhabditis elegans* adult germ line. Mol Biol Cell 17, 3051–3061.

Crittenden SL, Seidel HS, Kimble J (2017). Analysis of the *C. elegans* germline stem cell pool. Methods Mol Biol 1463, 1–33.

Degirmenci B, Valenta T, Dimitrieva S, Hausmann G, Basler K (2018). GLI1-expressing mesenchymal cells form the essential Wnt-secreting niche for colon stem cells. Nature 558, 449–453.

Fox PM, Vought VE, Hanazawa M, Lee MH, Maine EM, Schedl T (2011). Cyclin E and CDK-2 regulate proliferative cell fate and cell cycle progression in the *C. elegans* germline. Development 138, 2223–2234.

Franca LR, Hess RA, Dufour JM, Hofmann MC, Griswold MD (2016). The Sertoli cell: one hundred fifty years of beauty and plasticity. Andrology 4, 189–212.

Frøkjær-Jensen C, Davis MW, Sarov M, Taylor J, Flibotte S, LaBella M, Pozniakovsky A, Moerman DG, Jorgensen EM (2014). Random and targeted transgene insertion in *Caenorhabditis elegans* using a modified *Mos1* transposon. Nat Methods 11, 529–534.

Furuta T, Tuck S, Kirchner J, Koch B, Auty R, Kitagawa R, Rose AM, Greenstein D (2000). EMB-30: An APC4 homologue required for metaphase-to-anaphase transitions during meiosis and mitosis in *Caenorhabditis elegans*. Mol Biol Cell 11, 1401–1419.

Gordon KL, Payne SG, Linden-High LM, Pani AM, Goldstein B, Hubbard EJA, Sherwood DR (2019). Ectopic germ cells can induce niche-like enwrapment by neighboring body wall muscle. Curr Biol 29, 823–833 e825.

Henderson ST, Gao D, Lambie EJ, Kimble J (1994). *lag-2* may encode a signaling ligand for the GLP-1 and LIN-12 receptors of *C. elegans*. Development 120, 2913–2924.

Hendzel MJ, Wei Y, Mancini MA, Van Hooser A, Ranalli T, Brinkley BR, Bazett-Jones DP, Allis CD (1997). Mitosis-specific phosphorylation of histone H3 initiates primarily within pericentromeric heterochromatin during G2 and spreads in an ordered fashion coincident with mitotic chromosome condensation. Chromosoma 106, 348–360.

Hirsh D, Oppenheim D, Klass M (1976). Development of the reproductive system of *Caenorhabditis elegans*. Dev Biol 49, 200–219.

Huang H, Kornberg TB (2015). Myoblast cytonemes mediate Wg signaling from the wing imaginal disc and Delta-Notch signaling to the air sac primordium. Elife 4, e06114.

Jeong J, Verheyden JM, Kimble J (2011). Cyclin E and Cdk2 control GLD-1, the mitosis/meiosis decision, and germline stem cells in *Caenorhabditis elegans*. PLoS Genet 7, e1001348.

Jones DL, Wagers AJ (2008). No place like home: anatomy and function of the stem cell niche. Nat Rev Mol Cell Biol 9, 11–21.

Kapp FG, Perlin JR, Hagedorn EJ, Gansner JM, Schwarz DE, O'Connell LA, Johnson NS, Amemiya C, Fisher DE, Wolfle U, *et al.* (2018). Protection from UV light is an evolutionarily conserved feature of the haematopoietic niche. Nature 558, 445–448.

Kelly WG, Xu S, Montgomery MK, Fire A (1997). Distinct requirements for somatic and germline expression of a generally expressed *Caernorhabditis elegans* gene. Genetics 146, 227–238.

Kershner AM, Shin H, Hansen TJ, Kimble J (2014). Discovery of two GLP-1/Notch target genes that account for the role of GLP-1/Notch signaling in stem cell maintenance. Proc Natl Acad Sci USA 111, 3739–3744.

Kimble JE, White JG (1981). On the control of germ cell development in *Caenorhabditis elegans*. Dev Biol 81, 208–219.

Komatsu H, Chao MY, Larkins-Ford J, Corkins ME, Somers GA, Tucey T, Dionne HM, White JQ, Wani K, Boxem M, Hart AC (2008). OSM-11 facilitates LIN-12 Notch signaling during *Caenorhabditis elegans* vulval development. PLoS Biol 6, e196.

Kostas SA, Fire A (2002). The T-box factor MLS-1 acts as a molecular switch during specification of nonstriated muscle in *C. elegans*. Genes Dev 16, 257–269.

Kovall RA, Gebelein B, Sprinzak D, Kopan R (2017). The canonical Notch signaling pathway: Structural and biochemical insights into shape, sugar, and force. Dev Cell 41, 228–241.
Lander AD, Kimble J, Clevers H, Fuchs E, Montarras D, Buckingham M, Calof AL, Trumpp A, Oskarsson T (2012). What does the concept of the stem cell niche really mean today? BMC Biol 10, 19.
Lee C, Seidel HS, Lynch TR, Sorensen EB, Crittenden SL, Kimble J (2017). Single-molecule RNA fluorescence *in situ* hybridization (smFISH) in *Caenorhabditis elegans*. Bio-protocol 7, e2357.
Lee C, Sorensen EB, Lynch TR, Kimble J (2016). *C. elegans* GLP-1/Notch activates transcription in a probability gradient across the germline stem cell pool. Elife 5, e18370.
Linden LM, Gordon KL, Pani AM, Payne SG, Garde A, Burkholder D, Chi Q, Goldstein B, Sherwood DR (2017). Identification of regulators of germ stem cell enwrapment by its niche in *C. elegans*. Dev Biol 429, 271–284.
Luca VC, Kim BC, Ge C, Kakuda S, Wu D, Roein-Peikar M, Haltiwanger RS, Zhu C, Ha T, Garcia KC (2017). Notch-Jagged complex structure implicates a catch bond in tuning ligand sensitivity. Science 355, 1320–1324.
Maciejowski J, Ugel N, Mishra B, Isopi M, Hubbard EJA (2006). Quantitative analysis of germline mitosis in adult *C. elegans*. Dev Biol 292, 142–151.
Morgan DE, Crittenden SL, Kimble J (2010). The *C. elegans* adult male germline: Stem cells and sexual dimorphism. Dev Biol 346, 204–214.
Nadarajan S, Govindan JA, McGovern M, Hubbard EJA, Greenstein D (2009). MSP and GLP-1/Notch signaling coordinately regulate actomyosin-dependent cytoplasmic streaming and oocyte growth in *C. elegans*. Development 136, 2223–2234.
Pekar O, Ow MC, Hui KY, Noyes MB, Hall SE, Hubbard EJA (2017). Linking the environment, DAF-7/TGFβ signaling and LAG-2/DSL ligand expression in the germline stem cell niche. Development 144, 2896–2906.
Raiders SA, Eastwood MD, Bacher M, Priess JR (2018). Binucleate germ cells in *Caenorhabditis elegans* are removed by physiological apoptosis. PLoS Genet 14, e1007417.
Rosu S, Cohen-Fix O (2017). Live-imaging analysis of germ cell proliferation in the *C. elegans* adult supports a stochastic model for stem cell proliferation. Dev Biol 423, 93–100.
Sallee MD, Littleford HE, Greenwald I (2017). A bHLH code for sexually dimorphic form and function of the *C. elegans* somatic gonad. Curr Biol 27, 1853–1860 e1855.
Schindelin J, Arganda-Carreras I, Frise E, Kaynig V, Longair M, Pietzsch T, Preibisch S, Rueden C, Saalfeld S, Schmid B, *et al.* (2012). Fiji: an open-source platform for biological-image analysis. Nat Methods 9, 676–682.
Seidel HS, Smith TA, Evans JK, Stamper JQ, Mast TG, Kimble J (2018). *C. elegans* germ cells divide and differentiate in a folded tissue. Dev Biol 442, 173–187.
Shin H, Haupt KA, Kershner AM, Kroll-Conner P, Wickens M, Kimble J (2017). SYGL-1 and LST-1 link niche signaling to PUF RNA repression for stem cell maintenance in *Caenorhabditis elegans*. PLoS Genet 13, e1007121.
Shoshkes-Carmel M, Wang YJ, Wangensteen KJ, Toth B, Kondo A, Massasa EE, Itzkovitz S, Kaestner KH (2018). Subepithelial telocytes are an important source of Wnts that supports intestinal crypts. Nature 557, 242–246.
Song X, Zhu CH, Doan C, Xie T (2002). Germline stem cells anchored by adherens junctions in the *Drosophila* ovary niches. Science 296, 1855–1857.
Spéder P, Brand AH (2018). Systemic and local cues drive neural stem cell niche remodelling during neurogenesis in *Drosophila*. Elife 7, e30413.
Spradling A, Fuller MT, Braun RE, Yoshida S (2011). Germline stem cells. Cold Spring Harb Perspect Biol 3, a002642.
Tamplin OJ, Durand EM, Carr LA, Childs SJ, Hagedorn EJ, Li P, Yzaguirre AD, Speck NA, Zon LI (2015). Hematopoietic stem cell arrival triggers dynamic remodeling of the perivascular niche. Cell 160, 241–252.
Visvader JE, Clevers H (2016). Tissue-specific designs of stem cell hierarchies. Nat Cell Biol 18, 349–355.
Wong BG, Paz A, Corrado MA, Ramos BR, Cinquin A, Cinquin O, Hui EE (2013). Live imaging reveals active infiltration of mitotic zone by its stem cell niche. Integr Biol (Camb) 5, 976–982.
Zhao J, Wang P, Corsi AK (2007). The *C. elegans* Twist target gene, *arg-1*, is regulated by distinct E box promoter elements. Mech Dev 124, 377–389.